Pressure-induced creation and annihilation of Weyl points in $T_d\text{-}Mo_{0.5}W_{0.5}Te_2$ and $1T''\text{-}Mo_{0.5}W_{0.5}Te_2$

Bishnu Karki, Bishnu Prasad Belbase, Gang Bahadur Acharya, Sobhit Singh, and Madhav Prasad Ghimire

Pressure-induced creation and annihilation of Weyl points in T_d-Mo$_{0.5}$W$_{0.5}$Te$_2$ and $1T''$-Mo$_{0.5}$W$_{0.5}$Te$_2$

Bishnu Karki,[1, *] Bishnu Prasad Belbase,[1, *] Gang Bahadur
Acharya,[1, 2] Sobhit Singh,[3, †] and Madhav Prasad Ghimire[1, 2, ‡]

[1]*Central Department of Physics, Tribhuvan University, Kirtipur, 44613, Kathmandu, Nepal*
[2]*Institute for Theoretical Solid State Physics, IFW Dresden, Helmholtzstr. 20, 01069 Dresden, Germany*
[3]*Department of Physics and Astronomy, Rutgers University, Piscataway, New Jersey 08854, USA*

By means of first-principles density-functional theory calculations, we investigate the role of hydrostatic pressure on the electronic structure of T_d ($Pmn2_1$) and $1T''$ (Pm) phases of Weyl semimetal Mo$_{0.5}$W$_{0.5}$Te$_2$, which is a promising material for phase-change memory technology and superconductivity. We particularly focus on changes occurring in the distribution of the gapless Weyl points (WPs) within 0 to 45 GPa pressure range. We further investigate the structural phase transition and lattice dynamics of the T_d and $1T''$ phases within the aforementioned pressure range. Our calculations suggest that both the T_d and $1T''$ phases of Mo$_{0.5}$W$_{0.5}$Te$_2$ host four WPs in their full Brillouin zone at zero pressure. The total number of WPs increases to 44 (36) with increasing pressure *via* pair creation up to 20 (15) GPa for the T_d ($1T''$) phase, and beyond this pressure pair annihilation of WPs starts occurring leaving only 16 WPs at 45 GPa in both phases. The enthalpy versus pressure data reveal that the $1T''$ phase is more favorable below the critical pressure of 7.5 GPa, however, beyond this critical pressure the T_d phase becomes enthalpically favorable. We also provide the calculated x-ray diffraction spectra along with the calculated Raman- and infrared-active phonon frequencies to facilitate the experimental identification of the studied phases.

I. INTRODUCTION

The study of topological materials is of high interest at present due to their potential applications in the emerging technology [1–9]. Weyl semimetals (WSMs), one class of topological materials, seem to drag special attention since their experimental realization in 2015 [10–15]. Breaking of either time-reversal symmetry or spatial inversion-symmetry, or both, in WSMs results in a particular electronic band structure possessing crossings of the nondegenerate valance and conduction bands near the Fermi level (E_F) forming gapless Weyl points (WPs) and Weyl cones [16]. The low-energy electronic excitations near these WPs behave as the massless Weyl fermions [17–25]. WSMs are interesting due to their exotic properties such as WPs acting as the sources and sinks of the Berry curvature in momentum space, existence of open Fermi-arc states connecting two opposite WPs, extremely large magnetoresistance [26–29], and various quantum Hall phenomena [30–37]. Moreover, based on the tilting of the band crossings near the Fermi level (E_F) two types of WSMs are reported: (i) type-I WSMs that preserve the Lorentz invariance and their Fermi surface shrinks to zero when the E_F is set at the energy of the WPs, and (ii) type-II WSMs that violate the Lorentz invariance due to peculiar tilting of the Weyl cone such that WPs occur at the touching points of an electron and hole pockets and the Fermi surface never shrinks to absolute zero when E_F is set at the energy of the WPs [3, 20, 22, 38–40].

WSMs belonging to the transition metal dichalcogenides (TMDs) family are special, mainly because the s, p, and d orbitals in these systems hybridize to form bands near the Fermi level, which often yield various fascinating properties such as distinct quantum phase transitions between different structures, thermal and optical properties, topological domain walls, different kinds of Hall effects, and superconductivity [41–47]. Notably, dome-shaped superconducting behaviour is observed in MoTe$_2$ with a transition temperature of 0.01 K that enhances to 8.2 K at 11.7 GPa pressure [45, 48–51]. MoTe$_2$ and WTe$_2$ are among the first reported WSMs with four WPs in their momentum space due to the broken inversion symmetry [52–64]. The application of external pressure and strain has been reported to play a vital role in tuning the WSM phase in MoTe$_2$ and WTe$_2$ [65–68].

Substitution of W by Mo in WTe$_2$, forming a polymorphic structure of Mo$_x$W$_{1-x}$Te$_2$, is reported to control the structural phase transition, transport properties, thermal conductivity, Weyl phase, and superconductivity in this system [69–76]. Depending on the magnitude of the applied pressure on Mo$_x$W$_{1-x}$Te$_2$ ($x = 0.9$, 0.6, and 0.25), the superconducting transition temperature can be tuned [77]. Moreover, tunable WSM phase and Fermi-arc states can be realized in Mo$_x$W$_{1-x}$Te$_2$ ($x \leq 0.5$) by varying x [78–80]. By means of the temperature-dependent elastic neutron scattering measurements, Schneeloch *et al.* [74] recently investigated the monoclinic $1T'$ to orthorhombic T_d structural phase transition in Mo$_{1-x}$W$_x$Te$_2$ as a function of the W substitution and temperature. They observed that $1T'$ – T_d phase transition is accompanied by an intermediate pseudo-orthorhombic phase T_d^*, which was first reported by Tao *et al.* [76] for pure MoTe$_2$. Notably, the intermediate T_d^* phase exists only up to $x = 0.34$ concentration and

vanishes for $x > 0.34$. Their results further suggest that at room temperature $Mo_{0.5}W_{0.5}Te_2$ composition favors the T_d phase [74]. Marchenkov *et al.* [75] experimentally studied the transport and optical properties of a single crystal $Mo_{0.5}W_{0.5}Te_2$. Their temperature-dependent resistivity data reveal the metallic nature of the system. Li *et al.* recently performed dimensionality-dependent transport measurements on a special $Mo_{0.5}W_{0.5}Te_2$ sample having a thickness gradient across 2D and 3D regimes and reported strong evidences that this material is a type-II WSM [81].

The experimental observation of pressure-controlled superconductivity in $Mo_{0.5}W_{0.5}Te_2$ [77] calls for a systematic investigation of the pressure-induced changes occurring in the crystal structure, electronic structure, and WSM phase of this system. In this work, we theoretically study the structural, vibrational, and topological electronic properties of $Mo_{0.5}W_{0.5}Te_2$ as a function of the hydrostatic pressure within 0 to 45 GPa pressure range. We explore the aforementioned properties of two candidate crystal phases of $Mo_{0.5}W_{0.5}Te_2$, T_d and $1T''$, as a function of the applied pressure. Our calculations indicate that both these phases are dynamically stable within the studied pressure range and both of them host a number of WPs in their momentum-energy space. Interestingly, WPs in both phases can be created *via* pair-creation, destroyed *via* pair-annihilation, and shifted in the momentum-energy space by application of an external pressure. Such a tunability of Weyl phase is desired for harnessing various transport and optical properties of WSMs [2–4, 82–85], particularly associated to the nonzero Berry-curvature dipole such as nonlinear Hall effect [86, 87], circular photogalvanic effect (CPGE) [88–90], and nonlinear optical responses [90–92]. Furthermore, creation/annihilation of WPs near the Fermi level as well as their shifting in the momentum-energy space can enhance/suppress electronic transport properties in WSMs. Our work implies that $Mo_{0.5}W_{0.5}Te_2$ inherits a variety of interesting topological properties at higher pressures and it may provide a novel platform for realization of Weyltronics. Furthermore, our results suggest an increase in the superconducting transition temperature at higher pressures, which is in agreement with recent experimental observations [44, 77].

II.   COMPUTATIONAL DETAILS

The density-functional theory (DFT) calculations were performed using the Projector Augmented Wave (PAW) method as implemented in the Vienna Ab initio Simulation Package (VASP) [93–95]. Six valence electrons were considered in the PAW pseudopotentials of Mo, W, and Te. The Perdew-Burke-Ernzerhof generalized-gradient approximation (GGA-PBE) was used to compute the exchange-correlation functional [96]. The GGA-opt86b functional was used for the van der Waals (vdW) density-functional corrections [97–99]. The reciprocal space was

sampled using a Γ-centered k-mesh of size $8 \times 12 \times 4$ together with a kinetic energy cutoff of 600 eV for plane waves. The energy and force convergence criteria were set to 10^{-8} eV and 10^{-4} eV/Å, respectively. The hydrostatic pressure was applied up to 45 GPa. The crystal structures were fully optimized in inner coordinates as well in cell parameters for each pressure considering spin-orbit coupling (SOC) and GGA-opt86b vdW corrections [97–99]. All the DFT calculations were carried out in a twelve-atom unit cell of $Mo_{0.5}W_{0.5}Te_2$. The optimized lattice parameters for the T_d phase at zero pressure are $a = 6.301$, $b = 3.490$, and $c = 14.076$ Å, and cell angles are $\alpha = \beta = \gamma = 90°$, which are in excellent agreement with the experimental data reported in Ref. [74].

The phonon calculations were performed using the finite-difference approach using supercells of size $2 \times 3 \times 1$. SOC was considered in all phonon calculations. The PHONOPY [100] package was utilized to plot the phonon dispersions. The MECHELASTIC [101, 102] package was used to perform the equation of states (EOS) analyses using the enthaply versus pressure data. In order to understand the distribution of Weyl points in the momentum-energy space, we compute the real-space Wannier Hamiltonian using the full potential local orbital (FPLO) code version 18 [103]. We employed the above-mentioned DFT convergence parameter in all the FPLO calculations. The Wannier fitting was done using PYFPLO [103] module of the FPLO package considering Mo:$4d, 5s$, W:$5d, 6s$, and Te:$5s, 5p$ as the local orbitals basis. The PYPROCAR code [104] was used to investigate the DFT calculated electronic band structures and VESTA [105] software was used to draw the crystal structures.

III.   RESULTS AND DISCUSSION

I.   Crystal structures

In order to theoretically investigate the electronic structure of $Mo_{0.5}W_{0.5}Te_2$, we prepare two candidate crystal structures, as shown in Figs. 1(a,b), by taking the parent T_d phase (space group $Pmn2_1$) of WTe_2 and systematically substituting one W atom by one Mo atom in each vertically-stacked layer. There are two possible ways to carry out such a substitution. First, we consider a scenario in which the ordering of Mo and W atoms is reversed in the adjacent vertically-stacked layers, i.e., (Mo-W)$\cdots$(W-Mo)$\cdots$(Mo-W)$\cdots$. This results in a crystal structure belonging to the space group $Pmn2_1$ (no. 31), similar to the parent T_d phase, hence we call this structure the T_d phase. Note, this structure retains the vertical glide-mirror symmetry, as discussed in Ref. [37]. Also, this structure does not break the orthorhombic symmetry of the parent T_d structure after a free DFT relaxation.

Second, we consider a scenario in which ordering of the Mo and W atoms remains the same within the adjacent vertically-stacked layers, i.e., (Mo-W)$\cdots$(Mo-W)$\cdots$(Mo-W)$\cdots$. Such a configuration breaks the vertical glide-
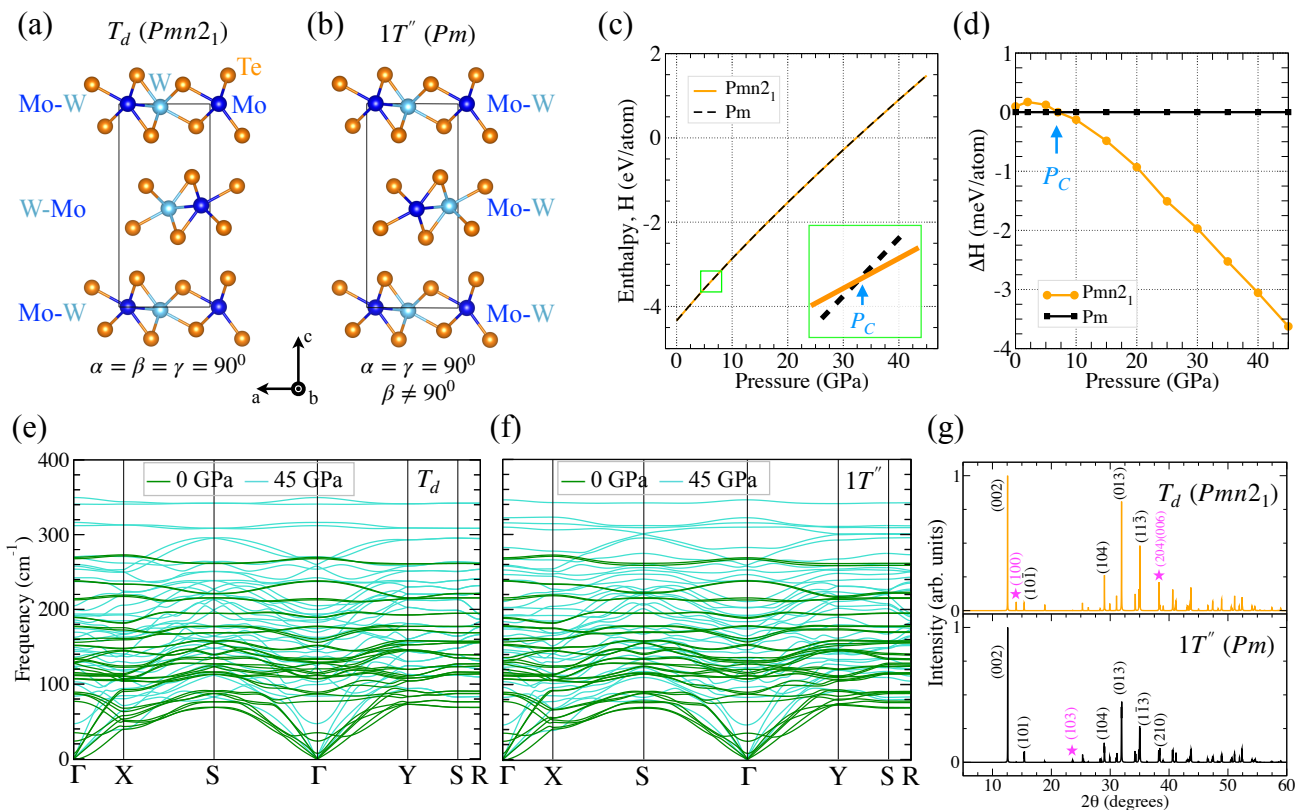
FIG. 1. (a, b) Crystal structures of the T_d and $1T''$ phases of $Mo_{0.5}W_{0.5}Te_2$. Note that $1T''$ has a subtle monoclinic distortion due to the cell angle $\beta \neq 90^0$. (c) Enthalpy versus pressure phase diagram for T_d and $1T''$ phases. The critical pressure (P_C) at which structural phase transition occurs is predicted near 7.5 GPa. Inset: an enlarged view near the crossing point. (d) The enthalpy difference ΔH ($= H_{T_d} - H_{1T''}$) as a function of pressure. (e, f) Calculated phonon spectra (with-SOC) at 0 and 45 GPa pressure for T_d and $1T''$ phases. We would like to note that we decided to plot the phonon dispersion for the $1T''$ phase along the same high-symmetry k-path as in the T_d phase for sake of better comparison, although $1T''$ phase has a subtle monoclinic distortion (see SM [106] for details). (g) The calculated x-ray diffraction (XRD) patterns for the T_d and $1T''$ phases at 0 GPa pressure. The signature peaks in both phases are marked using magenta color. More details of the crystal structures, calculated XRD patterns, phonon spectra calculated at higher pressures, and comparison of the calculated Raman-active phonon frequencies with the available experimental data are provided in the SM [106].

mirror symmetry [37] and results in the space group Pm (no. 6) after a free DFT relaxation of the unit cell. Note that the optimized structure is slightly distorted from the parent orthorhombic cell to a distorted monoclinic cell with a monoclinic cell angle of $\beta \neq 90°$, which varies as a function of the applied hydrostatic pressure, as we discuss below. Although this monoclinic structure is similar to the $1T'$ phase (space group: $P2_1/m$) of TMDs, it is lower in symmetry due to the broken inversion and vertical glide-mirror symmetries [37]. Therefore, we decide to call this monoclinic phase as the $1T''$ phase. We note both the structures, T_d and $1T''$, have broken inversion symmetry, which is a fundamental requirement for nonmagnetic Weyl semimetals.

Before moving further, let us briefly discuss the possible reason behind the observed monoclinic distortion in the $1T''$ phase. One could imagine the presence of an in-plane polarity orientation determined by the peculiar ordering of Mo and W atoms having different electronegativity within each vertically-stacked layer, as shown in

Figs. 1(a,b). In Fig. 1(a), where the ordering of Mo-W pairs is reversed as we move in the vertical direction, the in-plane polarity would reverse its sign in the adjacent vertically-stacked layers, i.e., $- + - + \cdots$ or $+ - + - \cdots$ (antipolar order). Here, $+/-$ sign denotes the polarity orientation parallel or antiparallel to the a lattice vector. In such a configuration, a free relaxation of structure does not require any monoclinic distortion of the orthorhombic cell due to the perfect cancellation of dipolar-like interactions along the vertical direction (not strictly speaking, because partial screening of electric dipoles may occur due to the semimetallic nature of this system). On the other hand, in Fig. 1(b), where the ordering of Mo-W pairs is the same in the adjacent vertical layers, the in-plane polarity would be parallel in the adjacent layers, i.e., $- - - - \cdots$ or $+ + + + \cdots$, similar to that of the $1T'$ phase [37, 47]. Hence, in order to minimize the total free energy such structures tend to exhibit a monoclinic distortion due to the sliding of the adjacent polar layers along the in-plane direction, as discussed in Ref. [37].

II.   Pressure-induced effects on the T_d and $1T''$ structures

Next, we test the relative stability of the T_d and $1T''$ phases as a function of pressure. Our calculations reveal that the enthalpy difference (ΔH) between these two phases is very small [Figs. 1(c, d)]. This implies the likelihood of formation of solid solution of the T_d and $1T''$ phases at finite temperatures. We find that below the critical pressure $(P_C = 7.5 \text{ GPa})$, the $1T''$ phase is more favorable, whereas above P_C the T_d phase is preferred. We further performed the EOS analyses using the Birch, Vinet, and Birch-Murnaghan models as implemented in the MECHELASTIC package [101, 107, 108]. The difference between the obtained EOS fitting parameters for the T_d and $1T''$ phases is minimal (see SM [106] for more details).

The phonon spectra calculated considering the SOC and vdW corrections for both the T_d [Fig. 1(e)] and $1T''$ [Fig. 1(f)] phases demonstrate the dynamical stability of these phases at zero pressure as well as at higher pressures (see SM [106]). We notice an increase in the phonon frequencies with increasing pressure, i.e., phonons harden at higher pressures. No dynamical instability was observed in both phases within the studied pressure range. A list of the infrared- and Raman-active phonon frequencies calculated at different pressures is provided in the SM [106]. We hope this could facilitate the experimental identification of the T_d and $1T''$ phases.

Furthermore, we calculate the x-ray diffraction (XRD) patterns of the T_d and $1T''$ phases at various pressures using Cu-Kα x-ray of wavelength 1.5406 Å. Fig. 1(g) shows the calculated XRD patterns at zero pressure (data at higher pressure are provided in SM [106]). Although the calculated XRD spectrum looks quite similar for both the phases, there are some signature peaks, marked using magenta stars, which are present in one phase but absent in another. These peaks can be used to distinguish between the T_d and $1T''$ phases in real crystals. Notably, the calculated peak position for the $(0\,0\,2)$ crystallographic peak and the Raman-active phonon frequencies (see SM [106]) match remarkably well with the reported experimental data for $Mo_{0.5}W_{0.5}Te_2$ single crystals [69].

Figs. 2(a,b) show the pressure dependence of the DFT optimized lattice parameters for T_d and $1T''$ phases. We observe a very similar trend in the pressure-dependent structural parameters of both phases. To highlight the observed trend, we plot the normalized the lattice parameters with respect to the lattice parameters obtained at zero pressure. We observe maximum change in the c lattice parameter with varying pressure. At 45 GPa, the c lattice parameter decreases by ~15% for both phases, whereas relative change in the a and b lattice parameters is less than 10% within the studied pressure range. Such a behavior is expected owing to the weak vdW interaction along the out-of-plane c axis. The optimized Mo-W bond length shows a similar pressure-dependent behavior as the in-plane lattice parameters. The Mo-W
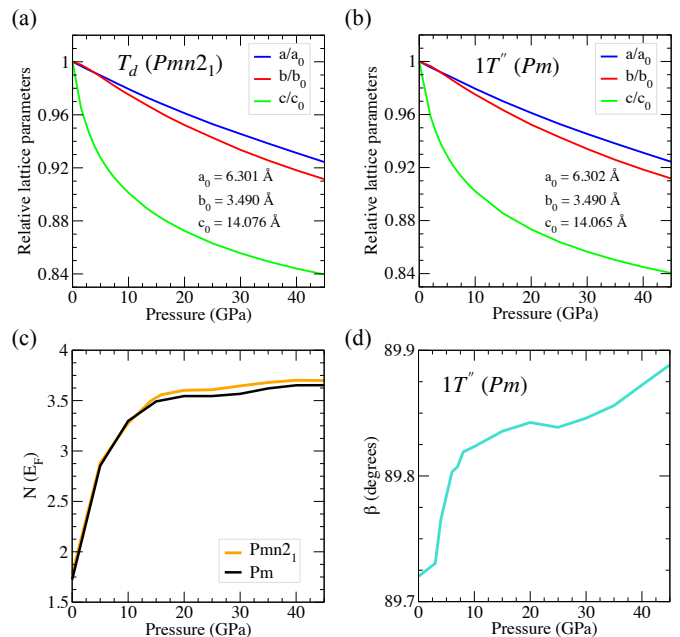

FIG. 2. (a, b) The optimized lattice parameters normalized to the lattice parameters obtained at zero pressure (a_0, b_0, c_0), and (c) the calculated density of states (states/eV) at the Fermi level N(E_F) plotted as a function of pressure for both T_d and $1T''$ phases. (d) Pressure-dependent variation in the monoclinic cell angle (β) for $1T''$ phase. Note that $\beta = 90^0$ for the T_d phase.

bond length decreases from a value 2.85 Å at zero pressure to 2.70 Å at 45 GPa. This is almost 5% decreases in the Mo-W bond length. On the other hand, the maximum compression in the Mo-Te and W-Te bond lengths is nearly 4% at 45 GPa.

Strikingly, the Te-Te interlayer distance undergoes the maximum change ($\sim 24\%$) as a function of external pressure in both the T_d and $1T''$ phases; the optimized Te-Te interlayer distance decreases from 3.93 Å at zero pressure to 2.98 Å at 45 GPa. Refs. [77, 109] pointed out that such a softening of the Te-Te interlayer vibrational mode substantially contributes to the overall electron-phonon coupling, which could possibly be the origin of the emergence of superconductivity in this system.

Fig. 2(d) shows the variation in the monoclinic angle β as a function of the pressure for the $1T''$ phase. With increasing pressure, the cell angle β tends to approach 90°, which implies a decrease in the monoclinic distortion and preference towards the orthorhombic T_d phase at higher pressures. This is consistent with the data shown in Fig. 1(d).

Since $Mo_{0.5}W_{0.5}Te_2$ is particularly interesting due to its superconducting properties [77], we calculate the density of states at the Fermi level N(E_F) as a function of pressure for both T_d and $1T''$ phases, as shown in Fig. 2(c). A systematic increase in N(E_F) with increasing pressure was observed in both phases. We would like to note that phonons also harden with increasing

pressure [see Figs. 1(e,f)]. Thus, an increased $N(E_F)$ together with the higher phonon frequencies implies an enhancement in the effective electron-phonon coupling at higher pressures, which could substantially increase the superconducting transition temperature in this system at higher pressures [48, 109–111]. This is consistent with recent experimental observations [44, 77].

III. Pressure-tunable Weyl semimetal phase

The band structure calculations of T_d and $1T''$ phase for different pressure is presented in Figs. 3 and 4. The topmost valence band indicated with green color forms hole pocket and bottom of the conduction band indicated with red color forms electron pocket nearby the E_F along the Γ-X, S-Γ-Y and U-Z-T high-symmetry directions of the Brillouin zone (BZ) [112]. These electron and the hole pockets touch each other at discrete points in the momentum space forming type-II WPs [52]. The change in pressure affects the size of the electron and hole pockets in the momentum space. With increasing pressure, these pockets come close to each other producing more number of band crossings, as implied in Figs. 3 and 4. A similar trend is found for the $1T''$ phase.

TMDs are the first class of materials to host type II WPs. Soluyanov *et al.* first reported type II WPs in pure WTe_2 located between 0.052 – 0.058 eV above E_F [52]. 16 WPs are found in the k- space with 8 WPs at $k_z = 0$ plane and 8 more WPs off the plane ($k_i \neq 0$, $i = x, y$ and z). With inclusion of SOC all the WPs at $k_i \neq 0$ are annihilated leaving only eight of the sixteen WPs. Similarly, Sun *et al.*, predicted the type II WSMs in $MoTe_2$ [61]. Eight WPs are recorded at two different energies 6 meV and 59 meV above E_F.

Here, in our study 50% substitution of Mo on WTe_2 without application of pressure, we report four WPs at an energy state 55 meV above the E_F at $k_z = 0$ plane for the T_d phase. Contrary to that, a similar number of WPs are recorded for the $1T''$ phase but at a different energy state of 93 meV below the E_F at $k_z \neq 0$ plane. The energy of the WPs obtained for the T_d phase is agreement with the energy of WPs for $MoTe_2$ [61] and WTe_2 [52], whereas the $1T''$ phase hosts WPs below E_F. Moreover, the chemical effect is also found to play a significant role for the change in the total number of the WPs in $Mo_{0.5}W_{0.5}Te_2$.

TABLE I. Location of W_1 WPs in the momentum space of the T_d and $1T''$ phases at zero pressure

WP	$k_x \left(\dfrac{2\pi}{a} \right)$	$k_y \left(\dfrac{2\pi}{b} \right)$	$k_z \left(\dfrac{2\pi}{c} \right)$	Chirality(χ)
$W_1(T_d)$	-0.132	-0.095	0.000	+1
$W_1(1T'')$	-0.004	-0.200	-0.416	+1

We obtain a total of four WPs (W_1) in the first BZ of the T_d and $1T''$ phases of $Mo_{0.5}W_{0.5}Te_2$ at zero pressure.

Co-ordinates of the nonequivalent W_1 WPs are given in Table I; other three WPs are the mirror reflections of W_1 at zero pressure. There is a variation in the total number and locations of the WPs due to the application of hydrostatic pressure. Below we discuss the role of the hydrostatic pressure on the Weyl phase of T_d- and $1T''$-$Mo_{0.5}W_{0.5}Te_2$.

a) Pressure effects on the T_d phase

The variation in the number of the WPs and their energy states for the T_d phase is presented through the graphical plots in Figs. 5 (a) and (b). On increasing the pressure value to 1.5 GPa the new sets of WPs W_2 and W_3 are generated along with the initial W_1 making the total number of WPs to 20. Here, we noticed that the pressure shifts the energy state of W_1 to E_F+75 meV. The newly created 8 copies of W_2 and W_3 are found in the energy states of E_F+8 meV and E_F-7 meV, respectively. No further creation of the WPs upto the pressure of 8 GPa, simply the position and the energy states of the WPs vary with the pressure. The energy state of W_1 rises to the highest value of E_F+139 meV at 8 GPa pressure and decreases on the further increase which reach nearest to the Fermi level (energy state E_F+1 meV) at 35 GPa and shifts below the Fermi level above that pressure. The pair creation of W_4 and W_5 each four in number occurs at 9 GPa which continue to exist up to 10 GPa and get annihilated above that pressure. The highest number of WPs is observed at 20 GPa and a constant number of 16 WPs is observed after 30 GPa to 45 GPa.

b) Pressure effects on the $1T''$ phase

Pressure also has an impact on the dynamics of WPs in the $1T''$ phase. Pair creation and the annihilation of WPs as the function of pressure is noticed in the momentum space of the $1T''$ phase. Here, the W_1 WPs continue to exist up to 10 GPa which annihilates on further rise in pressure. Similarly, the W_2 WPs are created at 5 GPa pressure, which exist up to 40 GPa and then get annihilated. A similar phenomenon of pair creation and annihilation is noticed for the other energy state of WPs as well, which is summarized in the Figs. 5 (c) and (d). As compared to the T_d phase more energy states of the WPs are observed in the $1T''$ phase due to its lower symmetry. In terms of the total number of WPs, the highest number 36 is observed at 15 GPa pressure, whereas a constant number of 16 WPs is noticed for pressure beyond 40 GPa.

IV. SUMMARY

In summary, we studied the structural, vibrational, electronic, and topological Weyl properties of $Mo_{0.5}W_{0.5}Te_2$ by means of first-principles DFT calculations. We find that there are two possible candidate structures, T_d and $1T''$, for 50:50 Mo:W substitution. We studied the aforementioned properties of these two
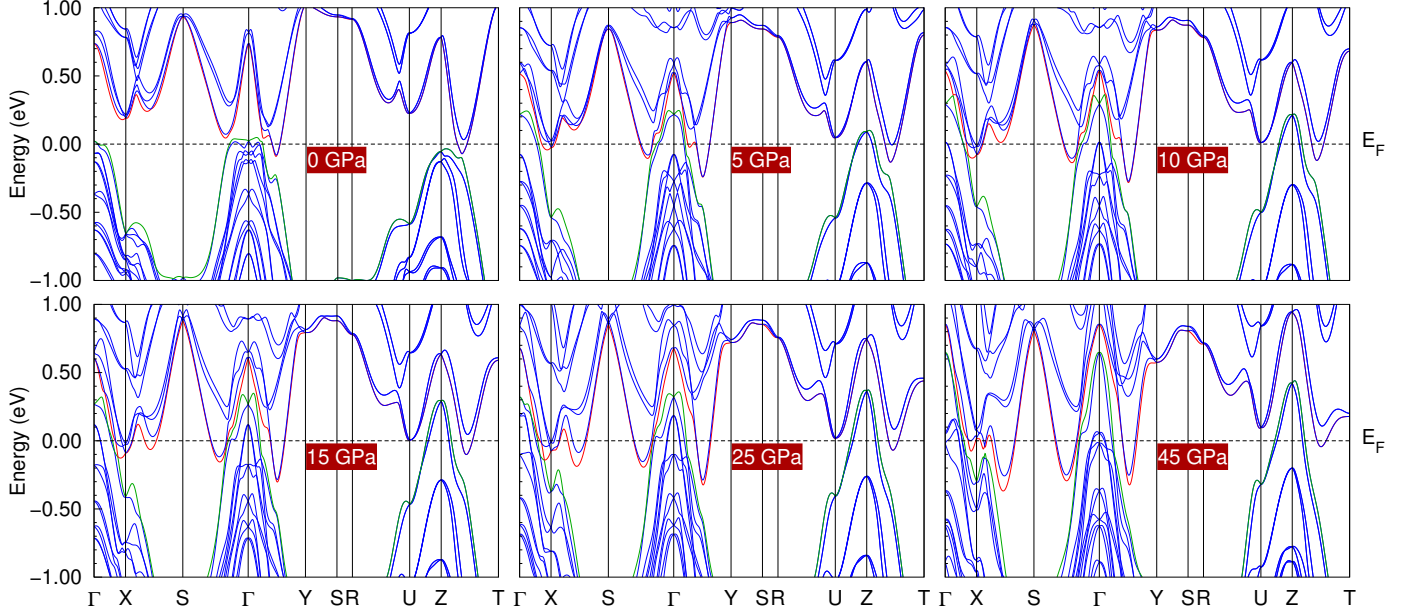
FIG. 3. Band structures of T_d phase calculated at pressure values of 0 GPa, 5 GPa, 10 GPa, 15 GPa, 25 GPa, and 45 GPa with inclusion of SOC. Red color in the band structure represents the lowest conduction band and the green color represents the highest valence band. The dashed horizontal line marks the E_F ($E_F = 0$ eV).
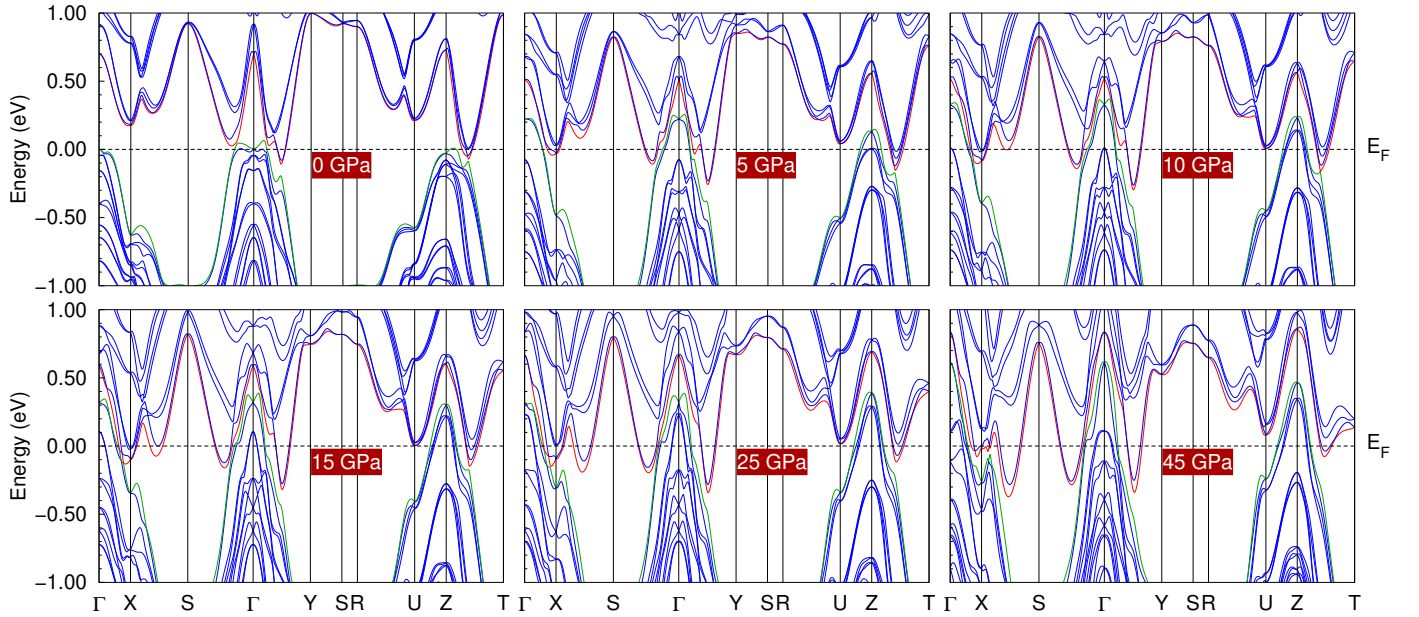

FIG. 4. Band structures of $1T''$ phase calculated at pressure values of 0 GPa, 5 GPa, 10 GPa, 15 GPa, 25 GPa, and 45 GPa with inclusion of SOC. Red color in the band structure represents the lowest conduction band and the green color represents the highest valence band. The dashed horizontal line marks the E_F. For the better comparison k paths of $1T''$ phase are also chosen same as in the T_d phase.

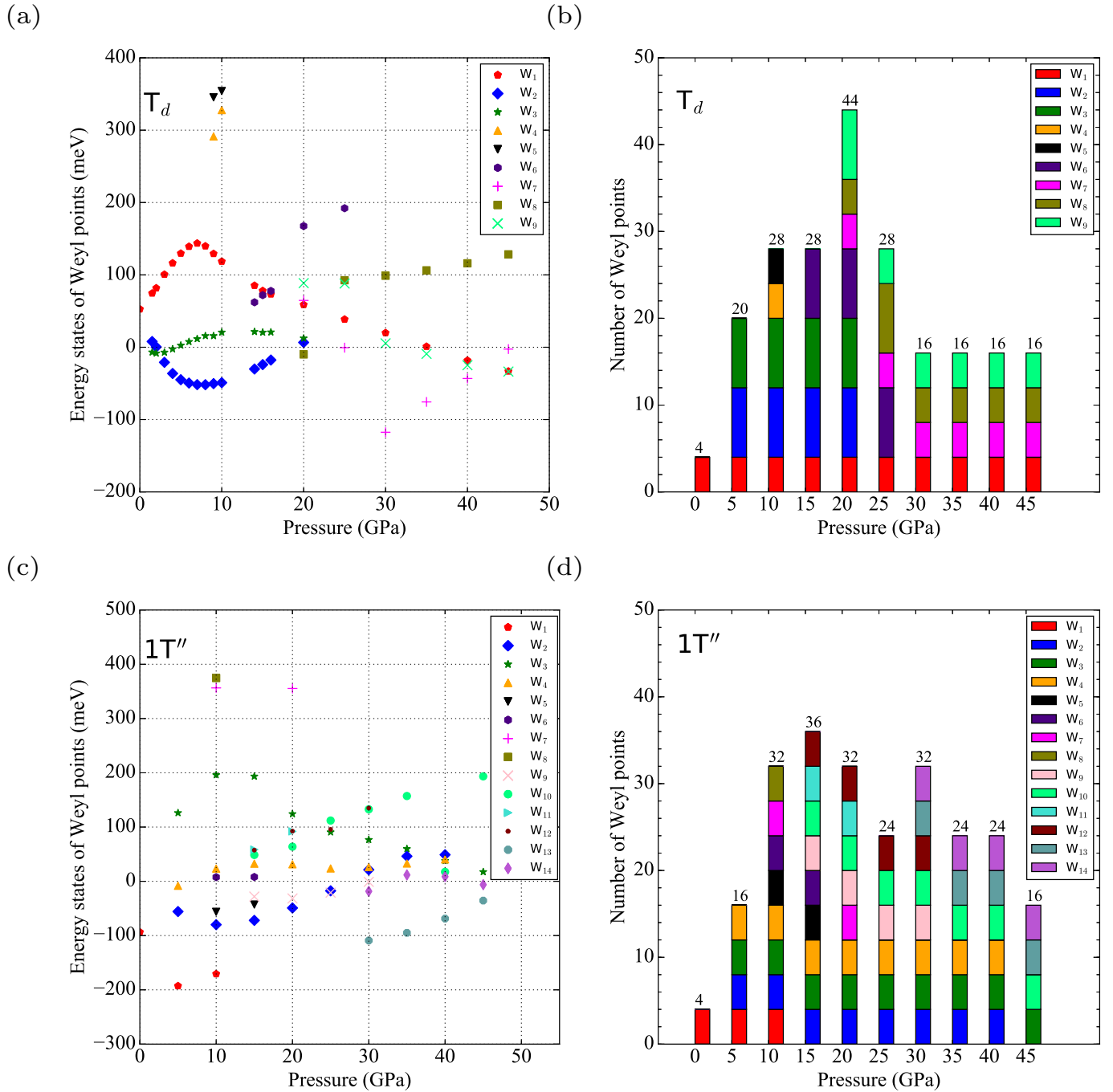phases in 0-45 GPa pressure range. We find that both these structures are energetically and dynamically stable

(a)

(b)

(c)

(d)

FIG. 5. (a) Energy states of WPs with respect to E_F calculated at different values of pressure for the T_d phase, (b) Stack-bar diagram showing the creation and annihilation of the WPs from 0 to 45 GPa for the T_d phase. (c) Energy states of WPs corresponding to different pressure for the $1T''$ phase. (d) Stack-bar diagram showing the creation and annihilation of the WPs from 0 to 45 GPa for the $1T''$ phase. The total number of WPs at each pressure is written at the top of each bar. See the SM [106] for more details regarding the number and location of WPs obtained at each pressure.

in the studied pressure. The calculated x-ray diffraction spectra, and the infrared- and Raman-active phonon frequencies indicate that these two phases can be identified in experiments, although they are likely to form solid solutions due to the subtle difference in their enthalpy at low pressures. The T_d ($1T''$) phase is theoretically more favorable at higher (lower) pressures, the critical pressure being 7.5 GPa. Our calculations reveal that the density of states and phonon frequencies increase dramatically with increasing pressure in both phases, which is indicative of

larger electron-phonon coupling at higher pressures and it could substantially increase the superconducting transition temperature in this system at higher pressures.

Interestingly, we find that both the T_d and $1T''$ phases host a number of WPs in their momentum-energy space. The total number and location of WPs can be controlled by varying hydrostatic pressure. Four WPs are obtained in the T_d and $1T''$ phases at zero pressure. The total number of WPs increases to 44 (36) with increasing pressure, via pair creation, up to 20 (15) GPa for the T_d ($1T''$) phase, and beyond this pressure, pair annihilation of WPs starts occurring leaving only 16 WPs at 45 GPa in both phases. Therefore, we can conclude that pressure can tune WPs to the desired location, generate new WPs, and also annihilate them, thus, providing an ideal platform for realization of Weyltronics in $Mo_{0.5}W_{0.5}Te_2$.

[1] M. Z. Hasan and C. L. Kane, Rev. Mod. Phys. **82**, 3045 (2010).

[2] N. P. Armitage, E. J. Mele, and A. Vishwanath, Rev. Mod. Phys. **90**, 015001 (2018).

[3] B. Yan and C. Felser, Annu. Rev. Condens. Matter Phys. **8**, 337 (2017).

[4] K. Manna, Y. Sun, L. Muechler, J. Kübler, and C. Felser, Nat. Rev. Mater. **3**, 244 (2018).

[5] H. Weng, X. Dai, and Z. Fang, J. Condens. Matter Phys. **28**, 303001 (2016).

[6] H. Gao, J. W. Venderbos, Y. Kim, and A. M. Rappe, Annu. Rev. Mater. **49**, 153 (2019).

[7] A. Burkov, Annu. Rev. Condens. Matter Phys. **9**, 359 (2018).

[8] M. Z. Hasan, S.-Y. Xu, I. Belopolski, and S.-M. Huang, Annu. Rev. Condens. Matter Phys. **8**, 289 (2017).

[9] M. Kang, L. Ye, S. Fang, J.-S. You, A. Levitan, M. Han, J. I. Facio, C. Jozwiak, A. Bostwick, E. Rotenberg, M. K. Chan, R. D. McDonald, D. Graf, K. Kaznatcheev, E. Vescovo, D. C. Bell, E. Kaxiras, J. van den Brink, M. Richter, M. Prasad Ghimire, J. G. Checkelsky, and R. Comin, Nature Materials **19**, 163 (2020).

[10] B. Lv, N. Xu, H. Weng, J. Ma, P. Richard, X. Huang, L. Zhao, G. Chen, C. Matt, F. Bisti, *et al.*, Nat. Phys. **11**, 724 (2015).

[11] B. Lv, H. Weng, B. Fu, X. Wang, H. Miao, J. Ma, P. Richard, X. Huang, L. Zhao, G. Chen, *et al.*, Phys. Rev. X **5**, 031013 (2015).

[12] S.-M. Huang, S.-Y. Xu, I. Belopolski, C.-C. Lee, G. Chang, B. Wang, N. Alidoust, G. Bian, M. Neupane, C. Zhang, *et al.*, Nat. Commun. **6**, 1 (2015).

[13] S.-Y. Xu, I. Belopolski, D. S. Sanchez, C. Zhang, G. Chang, C. Guo, G. Bian, Z. Yuan, H. Lu, T.-R. Chang, *et al.*, Sci. Adv. **1**, e1501092 (2015).

[14] A. B. Sushkov, J. B. Hofmann, G. S. Jenkins, J. Ishikawa, S. Nakatsuji, S. Das Sarma, and H. D. Drew, Phys. Rev. B **92**, 241108 (2015).

[15] B. Q. Lv, S. Muff, T. Qian, Z. D. Song, S. M. Nie, N. Xu, P. Richard, C. E. Matt, N. C. Plumb, L. X. Zhao, G. F. Chen, Z. Fang, X. Dai, J. H. Dil, J. Mesot, M. Shi, H. M. Weng, and H. Ding, Phys. Rev. Lett. **115**, 217601 (2015).

[16] S. Murakami, New J. Phys. **9**, 356 (2007).

[17] S. Jia, S.-Y. Xu, and M. Z. Hasan, Nat. Mater. **15**, 1140 (2016).

[18] H. Weyl, Z. Phys. **56**, 330 (1929).

[19] X. Wan, A. M. Turner, A. Vishwanath, and S. Y. Savrasov, Phys. Rev. B **83**, 205101 (2011).

[20] D. Grassano, O. Pulci, A. M. Conte, and F. Bechstedt, Sci. Rep. **8**, 1 (2018).

[21] J. Ruan, S.-K. Jian, H. Yao, H. Zhang, S.-C. Zhang, and D. Xing, Nat. Commun. **7**, 1 (2016).

[22] A. A. Soluyanov, D. Gresch, Z. Wang, Q. Wu, M. Troyer, X. Dai, and B. A. Bernevig, Nature **527**, 495 (2015).

[23] S. Singh, A. C. Garcia-Castro, I. Valencia-Jaime, F. Muñoz, and A. H. Romero, Phys. Rev. B **94**, 161116 (2016).

[24] S. Singh, Q. Wu, C. Yue, A. H. Romero, and A. A. Soluyanov, Phys. Rev. Mater. **2**, 114204 (2018).

[25] G. W. Winkler, S. Singh, and A. A. Soluyanov, Chin. Phys. B **28**, 077303 (2019).

[26] F. C. Chen, H. Y. Lv, X. Luo, W. J. Lu, Q. L. Pei, G. T. Lin, Y. Y. Han, X. B. Zhu, W. H. Song, and Y. P. Sun, Phys. Rev. B **94**, 235154 (2016).

[27] Q. L. Pei, W. J. Meng, X. Luo, H. Y. Lv, F. C. Chen, W. J. Lu, Y. Y. Han, P. Tong, W. H. Song, Y. B. Hou, Q. Y. Lu, and Y. P. Sun, Phys. Rev. B **96**, 075132 (2017).

[28] S. Thirupathaiah, R. Jha, B. Pal, J. S. Matias, P. K. Das, P. K. Sivakumar, I. Vobornik, N. C. Plumb, M. Shi, R. A. Ribeiro, and D. D. Sarma, Phys. Rev. B **95**, 241105 (2017).

[29] S. Lee, J. Jang, S.-I. Kim, S.-G. Jung, J. Kim, S. Cho, S. W. Kim, J. Y. Rhee, K.-S. Park, and T. Park, Sci. Rep. **8**, 13937 (2018).

[30] S.-Y. Xu, I. Belopolski, N. Alidoust, M. Neupane, G. Bian, C. Zhang, R. Sankar, G. Chang, Z. Yuan, C.-C. Lee, *et al.*, Science **349**, 613 (2015).

[31] N. Xu, H. Weng, B. Lv, C. E. Matt, J. Park, F. Bisti, V. N. Strocov, D. Gawryluk, E. Pomjakushina, K. Conder, *et al.*, Nat. Commun. **7**, 1 (2016).

[32] I. Belopolski, S.-Y. Xu, D. S. Sanchez, G. Chang, C. Guo, M. Neupane, H. Zheng, C.-C. Lee, S.-M. Huang,

G. Bian, N. Alidoust, T.-R. Chang, B. Wang, X. Zhang, A. Bansil, H.-T. Jeng, H. Lin, S. Jia, and M. Z. Hasan, Phys. Rev. Lett. **116**, 066802 (2016).

[33] A. Tamai, Q. S. Wu, I. Cucchi, F. Y. Bruno, S. Riccò, T. K. Kim, M. Hoesch, C. Barreteau, E. Giannini, C. Besnard, A. A. Soluyanov, and F. Baumberger, Phys. Rev. X **6**, 031021 (2016).

[34] G. Autès, D. Gresch, M. Troyer, A. A. Soluyanov, and O. V. Yazyev, Phys. Rev. Lett. **117**, 066402 (2016).

[35] W. Zhang, Q. Wu, L. Zhang, S.-W. Cheong, A. A. Soluyanov, and W. Wu, Phys. Rev. B **96**, 165125 (2017).

[36] M. P. Ghimire, J. I. Facio, J.-S. You, L. Ye, J. G. Checkelsky, S. Fang, E. Kaxiras, M. Richter, and J. van den Brink, Phys. Rev. Res. **1**, 032044 (2019).

[37] S. Singh, J. Kim, K. M. Rabe, and D. Vanderbilt, Phys. Rev. Lett. **125**, 046402 (2020).

[38] G. Autès, D. Gresch, M. Troyer, A. A. Soluyanov, and O. V. Yazyev, Phys. Rev. Lett. **117**, 066402 (2016).

[39] G. Chang, S.-Y. Xu, D. S. Sanchez, S.-M. Huang, C.-C. Lee, T.-R. Chang, G. Bian, H. Zheng, I. Belopolski, N. Alidoust, et al., Sci. Adv. **2**, e1600295 (2016).

[40] K. Koepernik, D. Kasinathan, D. V. Efremov, S. Khim, S. Borisenko, B. Büchner, and J. van den Brink, Phys. Rev. B **93**, 201101 (2016).

[41] B. Sipos, A. F. Kusmartseva, A. Akrap, H. Berger, L. Forró, and E. Tutiš, Nat. Mater. **7**, 960 (2008).

[42] X. Qian, J. Liu, L. Fu, and J. Li, Science **346**, 1344 (2014).

[43] R. Morris, R. Coleman, and R. Bhandari, Phys. Rev. B **5**, 895 (1972).

[44] H. Takahashi, T. Akiba, K. Imura, T. Shiino, K. Deguchi, N. K. Sato, H. Sakai, M. S. Bahramy, and S. Ishiwata, Phys. Rev. B **95**, 100501 (2017).

[45] Y. Qi, P. G. Naumov, M. N. Ali, C. R. Rajamathi, W. Schnelle, O. Barkalov, M. Hanfland, S.-C. Wu, C. Shekhar, Y. Sun, et al., Nat. Commun. **7**, 1 (2016).

[46] F. C. Chen, X. Luo, J. Yan, Y. Sun, H. Y. Lv, W. J. Lu, C. Y. Xi, P. Tong, Z. G. Sheng, X. B. Zhu, W. H. Song, and Y. P. Sun, Phys. Rev. B **98**, 041114 (2018).

[47] F.-T. Huang, S. Joon Lim, S. Singh, J. Kim, L. Zhang, J.-W. Kim, M.-W. Chu, K. M. Rabe, D. Vanderbilt, and S.-W. Cheong, Nat. Commun. **10**, 4211 (2019).

[48] C. Heikes, I.-L. Liu, T. Metz, C. Eckberg, P. Neves, Y. Wu, L. Hung, P. Piccoli, H. Cao, J. Leao, J. Paglione, T. Yildirim, N. P. Butch, and W. Ratcliff, Phys. Rev. Mater. **2**, 074202 (2018).

[49] R. C. Morris, R. V. Coleman, and R. Bhandari, Phys. Rev. B **5**, 895 (1972).

[50] H. Wei, S.-P. Chao, and V. Aji, Phys. Rev. B **89**, 014506 (2014).

[51] P. Hosur, X. Dai, Z. Fang, and X.-L. Qi, Phys. Rev. B **90**, 045130 (2014).

[52] A. A. Soluyanov, D. Gresch, Z. Wang, Q. Wu, M. Troyer, X. Dai, and B. A. Bernevig, Nature **527**, 495 (2015).

[53] P. Li, W. Wu, Y. Wen, C. Zhang, J. Zhang, S. Zhang, Z. Yu, S. A. Yang, A. Manchon, and X.-x. Zhang, Nat. Commun. **9**, 1 (2018).

[54] F. Y. Bruno, A. Tamai, Q. Wu, I. Cucchi, C. Barreteau, A. De La Torre, S. M. Walker, S. Riccò, Z. Wang, T. Kim, et al., Phys. Rev. B **94**, 121112 (2016).

[55] Y. Wu, D. Mou, N. H. Jo, K. Sun, L. Huang, S. L. Bud'ko, P. C. Canfield, and A. Kaminski, Phys. Rev.

B **94**, 121113 (2016).

[56] P. Li, Y. Wen, X. He, Q. Zhang, C. Xia, Z.-M. Yu, S. A. Yang, Z. Zhu, H. N. Alshareef, and X.-X. Zhang, Nat. Commun. **8**, 1 (2017).

[57] Y.-Y. Lv, X. Li, B.-B. Zhang, W. Deng, S.-H. Yao, Y. Chen, J. Zhou, S.-T. Zhang, M.-H. Lu, L. Zhang, et al., Phys. Rev. Lett. **118**, 096603 (2017).

[58] L. Huang, T. M. McCormick, M. Ochi, Z. Zhao, M.-T. Suzuki, R. Arita, Y. Wu, D. Mou, H. Cao, J. Yan, et al., Nat. Mater. **15**, 1155 (2016).

[59] K. Deng, G. Wan, P. Deng, K. Zhang, S. Ding, E. Wang, M. Yan, H. Huang, H. Zhang, Z. Xu, et al., Nat. Phys. **12**, 1105 (2016).

[60] M. Sakano, M. Bahramy, H. Tsuji, I. Araya, K. Ikeura, H. Sakai, S. Ishiwata, K. Yaji, K. Kuroda, A. Harasawa, et al., Phys. Rev. B **95**, 121101 (2017).

[61] Y. Sun, S.-C. Wu, M. N. Ali, C. Felser, and B. Yan, Phys. Rev. B **92**, 161107 (2015).

[62] Z. Wang, D. Gresch, A. A. Soluyanov, W. Xie, S. Kushwaha, X. Dai, M. Troyer, R. J. Cava, and B. A. Bernevig, Phys. Rev. Lett. **117**, 056805 (2016).

[63] J. Jiang, Z. Liu, Y. Sun, H. Yang, C. Rajamathi, Y. Qi, L. Yang, C. Chen, H. Peng, C. Hwang, et al., Nat. Commun. **8**, 13973 (2017).

[64] A. Liang, J. Huang, S. Nie, Y. Ding, Q. Gao, C. Hu, S. He, Y. Zhang, C. Wang, B. Shen, et al., arXiv:1604.01706 (2016).

[65] Y. Sun, S.-C. Wu, M. N. Ali, C. Felser, and B. Yan, Phys. Rev. B **92**, 161107 (2015).

[66] S. Dissanayake, C. Duan, J. Yang, J. Liu, M. Matsuda, C. Yue, J. A. Schneeloch, J. C. Y. Teo, and D. Louca, npj Quantum Mater. **4**, 45 (2019).

[67] N. Aryal and E. Manousakis, Phys. Rev. B **99**, 035123 (2019).

[68] N. Xu, Z. W. Wang, A. Magrez, P. Bugnon, H. Berger, C. E. Matt, V. N. Strocov, N. C. Plumb, M. Radovic, E. Pomjakushina, K. Conder, J. H. Dil, J. Mesot, R. Yu, H. Ding, and M. Shi, Phys. Rev. Lett. **121**, 136401 (2018).

[69] Y.-Y. Lv, L. Cao, X. Li, B.-B. Zhang, K. Wang, B. Pang, L. Ma, D. Lin, S.-H. Yao, J. Zhou, Y. B. Chen, S.-T. Dong, W. Liu, M.-H. Lu, Y. Chen, and Y.-F. Chen, Sci. Rep. **7**, 44587 (2017).

[70] X.-J. Yan, Y.-Y. Lv, L. Li, X. Li, S.-H. Yao, Y.-B. Chen, X.-P. Liu, H. Lu, M.-H. Lu, and Y.-F. Chen, Appl. Phys. Lett. **110**, 211904 (2017).

[71] S. M. Oliver, R. Beams, S. Krylyuk, I. Kalish, A. K. Singh, A. Bruma, F. Tavazza, J. Joshi, I. R. Stone, S. J. Stranick, et al., 2D Mater. **4**, 045008 (2017).

[72] D. Rhodes, D. A. Chenet, B. E. Janicek, C. Nyby, Y. Lin, W. Jin, D. Edelberg, E. Mannebach, N. Finney, A. Antony, T. Schiros, T. Klarr, A. Mazzoni, M. Chin, Y. c. Chiu, W. Zheng, Q. R. Zhang, F. Ernst, J. I. Dadap, X. Tong, J. Ma, R. Lou, S. Wang, T. Qian, H. Ding, R. M. Osgood, D. W. Paley, A. M. Lindenberg, P. Y. Huang, A. N. Pasupathy, M. Dubey, J. Hone, and L. Balicas, Nano Lett. **17**, 1616 (2017).

[73] O. B. Aslan, I. M. Datye, M. J. Mleczko, K. Sze Cheung, S. Krylyuk, A. Bruma, I. Kalish, A. V. Davydov, E. Pop, and T. F. Heinz, Nano Lett. **18**, 2485 (2018).

[74] J. A. Schneeloch, Y. Tao, C. Duan, M. Matsuda, A. A. Aczel, J. A. Fernandez-Baca, G. Xu, J. C. Neuefeind, J. Yang, and D. Louca, Phys. Rev. B **102**, 054105 (2020).

[75] V. Marchenkov, A. Domozhirova, A. Makhnev, E. Shreder, S. Naumov, V. Chistyakov, J. Huang, and M. Eisterer, Low Temp. Phys. **45**, 241 (2019).

[76] Y. Tao, J. A. Schneeloch, C. Duan, M. Matsuda, S. E. Dissanayake, A. A. Aczel, J. A. Fernandez-Baca, F. Ye, and D. Louca, Phys. Rev. B **100**, 100101 (2019).

[77] R. Dahal, L. Z. Deng, N. Poudel, M. Gooch, Z. Wu, H. C. Wu, H. D. Yang, C. K. Chang, and C. W. Chu, Phys. Rev. B **101**, 140505 (2020).

[78] I. Belopolski, S.-Y. Xu, Y. Ishida, X. Pan, P. Yu, D. S. Sanchez, H. Zheng, M. Neupane, N. Alidoust, G. Chang, et al., Phys. Rev. B **94**, 085127 (2016).

[79] T.-R. Chang, S.-Y. Xu, G. Chang, C.-C. Lee, S.-M. Huang, B. Wang, G. Bian, H. Zheng, D. S. Sanchez, I. Belopolski, et al., Nat. Commun. **7**, 1 (2016).

[80] I. Belopolski, D. S. Sanchez, Y. Ishida, X. Pan, P. Yu, S.-Y. Xu, G. Chang, T.-R. Chang, H. Zheng, N. Alidoust, et al., Nat. Commun. **7**, 1 (2016).

[81] P. Li, Y. Deng, C.-H. Hsu, C. Zhu, J. Cui, X. Yang, J. Zhou, Y.-C. Hung, J. Fan, Z. Ji, F. Qu, J. Shen, C. Yang, X. Jing, H. Lin, Z. Liu, L. Lu, and G. Liu, Phys. Rev. B **104**, 085423 (2021).

[82] B. Ramshaw, K. A. Modic, A. Shekhter, Y. Zhang, E.-A. Kim, P. J. Moll, M. D. Bachmann, M. Chan, J. Betts, F. Balakirev, et al., Nature communications **9**, 1 (2018).

[83] E. V. Gorbar, V. A. Miransky, I. A. Shovkovy, and P. O. Sukhachov, Low Temperature Physics **44**, 487 (2018).

[84] J. Hu, S.-Y. Xu, N. Ni, and Z. Mao, Annual Review of Materials Research **49**, 207 (2019), https://doi.org/10.1146/annurev-matsci-070218-010023.

[85] N. P. Ong and S. Liang, Nature Reviews Physics **3**, 394 (2021).

[86] I. Sodemann and L. Fu, Phys. Rev. Lett. **115**, 216806 (2015).

[87] Q. Ma, S.-Y. Xu, H. Shen, D. MacNeill, V. Fatemi, T.-R. Chang, A. M. Mier Valdivia, S. Wu, Z. Du, C.-H. Hsu, S. Fang, Q. D. Gibson, K. Watanabe, T. Taniguchi, R. J. Cava, E. Kaxiras, H.-Z. Lu, H. Lin, L. Fu, N. Gedik, and P. Jarillo-Herrero, Nature **565**, 337 (2019).

[88] F. de Juan, A. G. Grushin, T. Morimoto, and J. E. Moore, Nature Communications **8**, 15995 (2017).

[89] E. J. König, H.-Y. Xie, D. A. Pesin, and A. Levchenko, Phys. Rev. B **96**, 075123 (2017).

[90] Y. Zhang, H. Ishizuka, J. van den Brink, C. Felser, B. Yan, and N. Nagaosa, Phys. Rev. B **97**, 241118 (2018).

[91] G. Liu, *Nonlinear Optical Responses in Type-II Weyl Semimetals* (University of Pennsylvania, 2019).

[92] Q. Xu, Y. Zhang, K. Koepernik, W. Shi, J. van den Brink, C. Felser, and Y. Sun, npj Computational Materials **6**, 32 (2020).

[93] G. Kresse and J. Furthmüller, Phys. Rev. B **54**, 11169 (1996).

[94] G. Kresse and J. Furthmller, Comput. Mater. Sci. **6**, 15 (1996).

[95] G. Kresse and D. Joubert, Phys. Rev. B **59**, 1758 (1999).

[96] J. P. Perdew, A. Ruzsinszky, G. I. Csonka, O. A. Vydrov, G. E. Scuseria, L. A. Constantin, X. Zhou, and K. Burke, Phys. Rev. Lett. **100**, 136406 (2008).

[97] J. c. v. Klimeš, D. R. Bowler, and A. Michaelides, Phys. Rev. B **83**, 195131 (2011).

[98] T. Thonhauser, V. R. Cooper, S. Li, A. Puzder, P. Hyldgaard, and D. C. Langreth, Phys. Rev. B **76**, 125112 (2007).

[99] M. Dion, H. Rydberg, E. Schröder, D. C. Langreth, and B. I. Lundqvist, Phys. Rev. Lett. **92**, 246401 (2004).

[100] A. Togo and I. Tanaka, Scr. Mater. **108**, 1 (2015).

[101] S. Singh, L. Lang, V. Dovale-Farelo, U. Herath, P. Tavadze, F.-X. Coudert, and A. H. Romero, Comput. Phys. Commun. **267**, 108068 (2021).

[102] S. Singh, I. Valencia-Jaime, O. Pavlic, and A. H. Romero, Phys. Rev. B **97**, 054108 (2018).

[103] K. Koepernik and H. Eschrig, Phys. Rev. B **59**, 1743 (1999).

[104] U. Herath, P. Tavadze, X. He, E. Bousquet, S. Singh, F. Muñoz, and A. H. Romero, Comput. Phys. Commun. **251**, 107080 (2020).

[105] K. Momma and F. Izumi, J. Appl. Crystallogr. **44**, 1272 (2011).

[106] See Supplemental Material at [href] for a detailed information about the XRD spectra, phonon spectra, Raman- and infrared-active phonon frequencies, DOS, and distribution of WPs calculated at higher pressures.

[107] P. Vinet, J. Ferrante, J. H. Rose, and J. R. Smith, J. Geophys. Res. Solid Earth **92**, 9319 (1987).

[108] P. Vinet, J. H. Rose, J. Ferrante, and J. R. Smith, J. Condens. Matter Phys. **1**, 1941 (1989).

[109] P. Lu, J.-S. Kim, J. Yang, H. Gao, J. Wu, D. Shao, B. Li, D. Zhou, J. Sun, D. Akinwande, D. Xing, and J.-F. Lin, Phys. Rev. B **94**, 224512 (2016).

[110] R. Dynes, Solid State Commun. **10**, 615 (1972).

[111] H. Paudyal, S. Poncé, F. Giustino, and E. R. Margine, Phys. Rev. B **101**, 214515 (2020).

[112] W. Setyawan and S. Curtarolo, Comput. Mater. Sci. **49**, 299 (2010).